Upper and lower critical decay exponents of Ising ferromagnets with long-range interaction

Toshiki Horita,[1] Hidemaro Suwa,[2] and Synge Todo[2,3]

[1]*Department of Applied Physics, University of Tokyo, Tokyo 113-8656, Japan*
[2]*Department of Physics, University of Tokyo, Tokyo 113-0033, Japan*
[3]*Institute for Solid State Physics, University of Tokyo, Kashiwa 277-8581, Japan*

We investigate the universality class of the finite-temperature phase transition of the two-dimensional Ising model with the algebraically decaying ferromagnetic long-range interaction, $J_{ij} = |\vec{r}_i - \vec{r}_j|^{-(d+\sigma)}$, where d (=2) is the dimension of the system and σ is the decay exponent, by means of the order-N cluster-algorithm Monte Carlo method. In particular, we focus on the upper and lower critical decay exponents, the boundaries between the mean-field-universality, intermediate, and short-range-universality regimes. At the critical decay exponents, it is found that the standard Binder ratio of magnetization at the critical temperature exhibits extremely slow convergence as a function of the system size. We propose more effective physical quantities, namely the combined Binder ratio and the self-combined Binder ratio, both of which cancel the leading finite-size corrections of the conventional Binder ratio. Utilizing these techniques, we clearly demonstrate that in two dimensions, the lower and upper critical decay exponents are $\sigma = 1$ and 7/4, respectively, contrary to the recent Monte Carlo and renormalization-group studies [M. Picco, arXiv:1207.1018; T. Blanchard *et al.*, Europhys. Lett. **101**, 56003 (2013)].

I. INTRODUCTION

A system with long-range interaction can exhibit substantially different physics from the corresponding system with only short-range interaction [1–3]. Many materials show nontrivial phenomena in which the long-range nature of the interactions, such as the dipole-dipole interaction [4] and the Ruderman-Kittel-Kasuya-Yoshida (RKKY) interaction [5], plays an essential role. The competition between short-range and long-range interactions has been studied in cold-atom systems [6].

One of the simplest and most fundamental playgrounds for long-range interaction is the Ising model with the algebraically decaying interaction:

$$\mathcal{H} = -\sum_{i<j}^{N} J_{ij} S_i S_j, \tag{1}$$

where S_i (= ±1) is the Ising spin on the ith site, J_{ij} is the coupling constant between two spins (S_i and S_j), and N is the total number of spins. The summation in Eq. (1) runs over all spin pairs. The algebraically decaying ferromagnetic long-range interaction is expressed as

$$J_{ij} = \frac{1}{|\vec{r}_i - \vec{r}_j|^{d+\sigma}}, \tag{2}$$

where d is the dimension of the system, and $\vec{r}_i$ is the coordinate of the ith site on the square lattice. The decay exponent, σ, in Eq. (2) should be positive to ensure the extensiveness of the energy, i.e., finite energy density in the thermodynamic limit. Otherwise, one has to introduce an appropriate system-size-dependent normalization factor. The system with the algebraically decaying long-range interaction exhibits richer critical phenomena than those with only nearest-neighbor interaction. For sufficiently small σ, the finite-temperature phase transition is expected to belong to the mean-field universality class: in the limit of $d + \sigma \to 0$, the system becomes a fully connected model, or the Husimi-Temperley

model [7,8]. On the other hand, when σ is sufficiently large, the nearest-neighbor interaction dominates and the transition belongs to the short-range universality class. In the "intermediate regime" between the mean-field and the short-range limits, the critical exponents that characterize the universality class vary continuously [2,3]. For the d-dimensional system with the long-range interaction, this continuous change of the critical exponents between short-range and mean-field universalities can be interpreted as a continuous change of the effective dimension between d and the upper critical dimension of the corresponding short-range model. Although a number of theoretical and numerical studies [2,3,9–16] have been conducted in order to interpret the intermediate regime as nonintegral dimensions, precise identification between the decay exponent, σ, and the effective dimension has not been well established so far, in spite of the simple form of the Hamiltonian (1).

The main difficulty in precise estimation of the critical decay exponents is the strong (likely logarithmic) correction to scaling near the boundaries [2,15,17,18]. In the present paper, we propose two physical quantities, namely the combined Binder ratio and the self-combined Binder ratio, both of which cancel the leading corrections of the conventional Binder ratio. Using these combined Binder ratios, we investigate their universal ratio, the value at the critical point, as a function of the decay exponent (σ) precisely for the two-dimensional case. It is clarified that the lower and upper critical decay exponents are $\sigma = 1$ and 7/4, respectively.

The present paper is organized as follows: In the next section, the previous theoretical and numerical works on the present model are briefly reviewed. In Sec. III, we introduce the Fukui-Todo cluster-algorithm Monte Carlo method [19], which reduces the computational cost of simulating long-range interacting systems to $O(N)$. In Sec. IV, two physical quantities, namely the combined Binder ratio and the self-combined Binder ratio, are proposed together with the demonstration for the fully connected and the nearest-neighbor models. In Sec. V, we show our results of Monte Carlo simulations for model (1)

TABLE I. Critical exponents of the d-dimensional fully connected Ising model and the two-dimensional short-range Ising model [20].

	Fully connected	Short range
α	0 (discontinuous)	0 (log)
β	1/2	1/8
γ	1	7/4
δ	3	15
ν	2/d	1
η	$2 - d/2$	1/4

with coupling constant (2). Our study is concluded in Sec. VI. Details on the generalized Ewald-summation technique and the improved estimators are given, respectively, in Appendixes A and B.

II. SUMMARY OF PREVIOUS WORKS

The Ising model with the long-range interaction (2) has two limits: the fully connected Ising model $[(d + \sigma) \to 0]$ and the Ising model with only short-range interaction ($\sigma \to \infty$). The critical property of the phase transition in these limits is well established. The coupling constants of the former model are given by

$$J_{ij} = \frac{1}{N}. \tag{3}$$

On the other hand, those of the latter are

$$J_{ij} = \begin{cases} 1 & \text{if } i \text{ and } j \text{ are nearest neighbor,} \\ 0 & \text{otherwise.} \end{cases} \tag{4}$$

In Table I, the critical exponents of these models are summarized. Note that the critical exponents of the fully connected (mean-field) model depend on its dimension because its physical quantities scale with the total number of sites $N = L^d$ instead of the system length L. The well-known values $\nu = 1/2$ and $\eta = 0$ for the mean-field model are those at the upper critical dimension, i.e., $d = 4$.

A number of theoretical and numerical studies have been conducted mainly based on the renormalization-group (RG) argument and the Monte Carlo simulations. For the O(n) model with long-range interaction, Fisher *et al.* [2] performed the RG analysis. The O(n) model is a generalization of the Ising model ($n = 1$). They found three different regimes, depending on the value of the exponent σ as listed in Table II. In the intermediate regime, the critical exponent of the correlation function, η, varies linearly to σ. The results of their RG analysis have a flaw in that η at $\sigma = 2$, on the boundary between the intermediate

TABLE II. Renormalization-group prediction for the critical exponent η by Fisher *et al.* [2].

	σ	η
Mean-field regime	$\sigma < d/2$	1
Intermediate regime	$d/2 < \sigma < 2$	$2 - \sigma$
Short-range regime	$2 < \sigma$	η_{sr}

TABLE III. Renormalization-group prediction for the critical exponent η by Sak [3].

	σ	η
Mean-field regime	$\sigma < d/2$	1
Intermediate regime	$d/2 < \sigma < 2 - \eta_{sr}$	$2 - \sigma$
Short-range regime	$2 - \eta_{sr} < \sigma$	η_{sr}

regime and the short-range regime, is not determined uniquely. The exponent η becomes zero if one approaches $\sigma = 2$ from the side of the intermediate regime, while it becomes a finite value ($\eta_{sr} = 1/4$) in the short-range regime; thus, η changes discontinuously at $\sigma = 2$.

The boundary between the intermediate and the short-range regimes was more carefully considered by Sak [3] taking into account the higher-order terms in the RG calculations. In Ref. [3], it was concluded that the boundary is $\sigma = 2 - \eta_{sr}$ instead of $\sigma = 2$ as listed in Table III. Then, the exponent η becomes a continuous function of σ. Its derivative, nevertheless, is discontinuous at $\sigma = 2 - \eta_{sr}$ (and also at $\sigma = 1$).

Several theoretical studies have reported different conclusions. Most are based on the RG approach and the ϵ expansion of the Landau-Ginzburg effective Hamiltonian where the propagator contains the p^σ term in addition to the ordinary p^2 term. For example, van Enter [9] pointed out that the long-range perturbation is relevant for $2 - \eta_{sr} \leqslant \sigma \leqslant 2$ in contradiction to the result obtained by Sak [3].

In the meantime, the first numerical study of the Ising model with long-range interaction was reported by Luijten and Blöte [10]. By means of the cluster-algorithm Monte Carlo method, they calculated the exponent η for $d = 2$ as a function of σ, concluding that $\eta = 2 - \sigma$ up to $2 - \sigma = \eta_{sr}$ and $\eta = \eta_{sr} = 1/4$ for larger σ. This result seems consistent with the RG prediction by Sak [3]. Its error bar, however, is too large to exclude the possibility proposed by van Enter [9]. Recently, Picco [11] showed more precise Monte Carlo data than before and concluded that the exponent η varies smoothly, connecting the intermediate regime and the short-range regime, which disagrees with the previous RG analysis. Blanchard *et al.* [12] then supported the numerical result by means of the renormalization-group analysis with the double expansion. Nonetheless, another Monte Carlo calculation by Angelini *et al.* [15] and an RG study by Defenu *et al.* [16] agree with the result by Sak [3]. This discrepancy between the previous research has been an enigma for years.

III. MONTE CARLO METHOD FOR SYSTEMS WITH LONG-RANGE INTERACTION

The main difficulty in simulating a system with long-range interaction is the large calculation cost. The number of pairs is $N(N - 1)/2 \sim N^2$ for an N-spin system. A naive update in the Monte Carlo simulation will suffer from the $O(N^2)$ computational cost. To make matters worse, systems with long-range interaction are known for their egregious finite-size and boundary effects compared to the short-range model. Much larger systems thus need to be calculated, for the estimation of critical exponents, than in the case of

short-range interaction. In addition, it becomes important to take into account interactions from mirror-image cells across the periodic boundaries and the Ewald summation to further reduce the finite-size effect.

One of the first efficient algorithms for the Ising model with long-range interaction was proposed by Luijten and Blöte [21], whose computational cost scales in $O(N \log N)$. We will adopt the Fukui-Todo cluster algorithm [19], which is a more powerful approach; it further reduces the computational cost down to $O(N)$ for generic (unfrustrated) long-range interacting spin models [19,22,23].

The Fukui-Todo cluster algorithm is based on the Swendsen-Wang cluster algorithm [24]. In the original Swendsen-Wang algorithm for inverse temperature, β, we first activate each (interaction) bond with probability

$$P_{ij} = 1 - \exp(-2\beta J_{ij}) \qquad (5)$$

when $S_i = S_j$. Then spin clusters, each of which consists of spins connected by activated bonds, are flipped independently to generate the next spin configuration.

In the Fukui-Todo cluster algorithm, first we introduce the extended Fortuin-Kasteleyn representation [25,26]. The partition function of the Ising model (1) is rewritten as the extended Fortuin-Kasteleyn representation:

$$Z = \sum_{\{S_i\}} \sum_{\{k_{ij}\}} \prod_{i<j}^{N} \Delta(\sigma_{ij}, k_{ij}) V_{ij}(k_{ij}), \qquad (6)$$

where $\sigma_{ij} = S_i S_j$, and k_{ij} is a non-negative integer assigned to each spin pair (i,j). The "compatibility function" $\Delta(\sigma_{ij}, k_{ij})$ and the "weight" $V_{ij}(k_{ij})$ in Eq. (6) are defined as

$$\Delta(\sigma_{ij}, k_{ij}) = \begin{cases} 1 & \text{if } \sigma_{ij} = 1 \text{ or } k_{ij} = 0, \\ 0 & \text{otherwise,} \end{cases} \qquad (7)$$

and

$$V_{ij}(k_{ij}) = \frac{\exp(-2\beta J_{ij})(2\beta J_{ij})^{k_{ij}}}{k_{ij}!}, \qquad (8)$$

respectively. Due to the property of the compatibility function, the antiparallel spin configuration ($\sigma_{ij} = -1$) is prohibited when $k_{ij} \geqslant 1$. Then one can interpret a bond with $k_{ij} \geqslant 1$ and $k_{ij} = 0$ as an activated and deactivated bond, respectively, in a similar way to the original Swendsen-Wang algorithm. Note that $V_{ij}(k_{ij})$ is the probability mass function of the Poisson distribution with mean $2\beta J_{ij}$, and it satisfies the normalization condition $\sum_{k_{ij}=0}^{\infty} V_{ij}(k_{ij}) = 1$ for all (i,j).

Based on the generalized Fortuin-Kasteleyn representation (6), one Monte Carlo step of the Fukui-Todo cluster algorithm is performed as follows:

(i) Generate an integer k from the Poisson distribution $f(k; \lambda_{\text{tot}}) = \exp(-\lambda_{\text{tot}}) \lambda_{\text{tot}}^k / k!$, where $\lambda_{\text{tot}} = 2\beta \sum_{i<j}^{N} J_{ij}$.

(ii) Choose a pair (i,j) according to the probability $\lambda_{ij}/\lambda_{\text{tot}}$, and increase $k_{i,j}$ by 1 if $\sigma_{ij} = 1$, where $\lambda_{ij} = 2\beta J_{ij}$.

(iii) Repeat (ii) k times in total.

(iv) Spins connected by bonds with $k_{ij} > 0$ are considered to belong to the same cluster. Flip clusters at random and generate a new spin configuration as in the original Swendsen-Wang method.

The probability that bond (i,j) is activated can be expressed as

$$P_{ij} = \sum_{k=1}^{\infty} f(k; \lambda_{\text{tot}}) \sum_{m=1}^{k} \frac{k!}{(k-m)! m!} \left(\frac{\lambda_{ij}}{\lambda_{\text{tot}}} \right)^m$$

$$\times \left(1 - \frac{\lambda_{ij}}{\lambda_{\text{tot}}} \right)^{k-m}, \qquad (9)$$

since it is the probability that bond (i,j) is chosen at least once. By using the normalization condition

$$\sum_{m=0}^{k} \frac{k!}{(k-m)! m!} \left(\frac{\lambda_{ij}}{\lambda_{\text{tot}}} \right)^m \left(1 - \frac{\lambda_{ij}}{\lambda_{\text{tot}}} \right)^{k-m} = 1 \qquad (10)$$

of the binomial distribution, Eq. (9) can be rewritten as

$$P_{ij} = 1 - \sum_{k=0}^{\infty} f(k; \lambda_{\text{tot}}) \left(1 - \frac{\lambda_{ij}}{\lambda_{\text{tot}}} \right)^k$$

$$= 1 - \exp(-\lambda_{\text{tot}}) \sum_{k=0}^{\infty} \frac{1}{k!} (\lambda_{\text{tot}} - \lambda_{ij})^k$$

$$= 1 - \exp(-2\beta J_{ij}). \qquad (11)$$

That is, the activation probability in the Fukui-Todo method is equal to that in the original Swendsen-Wang algorithm (5). Thus both stochastic processes are equivalent to each other, satisfying the detailed balance.

The computational cost of the Fukui-Todo method is proportional to the repeat count, k, of step (ii). The average of k is λ_{tot}, obeying the Poisson distribution, $f(k, \lambda_{\text{tot}})$. For a system with N spins, λ_{tot} is expressed as

$$\lambda_{\text{tot}} = 2\beta \sum_{i<j}^{N} J_{ij} = \beta \sum_{i}^{N} \sum_{j \neq i}^{N} J_{ij}$$

$$\approx \beta \sum_{i}^{N} \int_{1}^{N^{1/d}} dr \, r^{d-1} J(r)$$

$$= \beta N \int_{1}^{N^{1/d}} dr \, r^{d-1} J(r). \qquad (12)$$

Here, we assume translational invariance and that J_{ij} depends only on the distance between spins. If $J(r)$ decays faster than r^{-d}, which is equivalent to the condition of the convergence of energy density for the ferromagnetic ordered state, the integral in the last line of Eq. (12) converges to a finite value even in the thermodynamic limit. The convergence condition is unchanged even when the mirror-image cells are considered and the Ewald summation is taken (see Appendix A). Thus, at a finite temperature, λ_{tot} increases in proportion to N instead of N^2 as long as $\sigma > 0$, and the energy density converges to a finite value. Because step (ii) is done in $O(1)$ computational cost thanks to Walker's method of alias (see the Appendixes of Ref. [19]), the total cost of one Monte Carlo step of the Fukui-Todo cluster algorithm is $O(\lambda_{\text{tot}}) \sim O(N)$.

IV. COMBINED BINDER RATIO

In the present work, instead of the critical exponents, we use the value of the Binder ratio to investigate the universality class

of the phase transition. The Binder ratio at the critical point, which is also referred to as the universal ratio, is constant and takes a universal value at the critical point [27], since it is the ratio of two physical quantities that have the same anomalous dimension at the critical point. It can usually be calculated more accurately than the critical exponents, which leads to more reliable identification of the universality class [28]. One of the simplest examples of such physical quantities is the so-called Binder ratio [27],

$$Q = \frac{\langle m^2 \rangle^2}{\langle m^4 \rangle}, \tag{13}$$

where $m = \sum_i S_i$ and $\langle \cdot \rangle$ denotes the Monte Carlo average.

In practice, the Binder ratio exhibits some system-size dependence that is called the correction to scaling. We write the Binder ratio at the critical temperature as follows:

$$Q(T_c, L) = Q_\infty + f(L), \tag{14}$$

where Q_∞ denotes the universal ratio and $f(L)$ does the finite-size correction. Note that the finite-size correction is not universal, i.e., it can be a different form even if the universality class is the same. Although it is generally difficult to know the explicit form of $f(L)$, the expression of the leading correction term is known for the fully connected Ising model [21]:

$$
\begin{aligned}
Q(T_c, N) &= \frac{\langle m^2 \rangle^2}{\langle m^4 \rangle} \\
&= 4\frac{\Gamma(3/4)^2}{\Gamma(1/4)^2} + \frac{16\sqrt{3}\Gamma(3/4)^3}{5\Gamma(1/4)^3} N^{-\frac{1}{2}} + O(N^{-1}),
\end{aligned}
\tag{15}
$$

where $\Gamma(x)$ is the gamma function. In the case of the two-dimensional fully connected Ising model ($N = L^2$), the leading correction is proportional to L^{-1}. One can consider different combinations of the moment of magnetization to build various "Binder ratios", whose universal ratio for the fully connected Ising model and its leading correction term at the critical point are also written explicitly as

$$\frac{\langle m^2 \rangle^3}{\langle m^6 \rangle} \simeq \frac{4\Gamma(3/4)^2}{3\Gamma(1/4)^2} + \left(\frac{4\sqrt{3}\Gamma(3/4)}{9\Gamma(1/4)} - \frac{16\sqrt{3}\Gamma(3/4)^3}{15\Gamma(1/4)^3}\right)N^{-\frac{1}{2}}, \tag{16}$$

$$\frac{\langle m^2 \rangle \langle m^4 \rangle}{\langle m^6 \rangle} \simeq \frac{1}{3} + \left(\frac{\sqrt{3}\Gamma(1/4)}{9\Gamma(3/4)} - \frac{8\sqrt{3}\Gamma(3/4)}{15\Gamma(1/4)}\right)N^{-\frac{1}{2}}, \tag{17}$$

$$\frac{\langle m^2 \rangle^4}{\langle m^8 \rangle} \simeq \frac{16\Gamma(3/4)^4}{5\Gamma(1/4)^4} + \frac{1536\sqrt{3}\Gamma(3/4)^5}{125\Gamma(1/4)^5} N^{-\frac{1}{2}}. \tag{18}$$

By using these Binder ratios, one can eliminate the lowest order of the correction to scaling. The simplest way to do this is to take an appropriate linear combination, e.g.,

$$C(T_c, N) = \frac{\langle m^2 \rangle^2}{\langle m^4 \rangle} - a\frac{\langle m^2 \rangle^3}{\langle m^6 \rangle} = C_{\text{MF}} + O(N^{-1}), \tag{19}$$

where

$$a = \frac{\frac{16\sqrt{3}\Gamma(3/4)^3}{5\Gamma(1/4)^3}}{\left(\frac{4\sqrt{3}\Gamma(3/4)}{9\Gamma(1/4)} - \frac{16\sqrt{3}\Gamma(3/4)^3}{15\Gamma(1/4)^3}\right)} \tag{20}$$

and $C_{\text{MF}} = 0.284\,344\,8$. Hereafter, we call $C(T, N)$ the combined Binder ratio.

Unfortunately, the construction of the combined Binder ratio requires an explicit form of the leading correction term. Application to other universality classes rather than the mean-field universality is not practical. Therefore, we introduce another quantity that also has smaller finite-size corrections, namely the "self-combined Binder ratio",

$$S(T, L) = \frac{1}{Q_\infty} Q(T, L) + Q_\infty \frac{1}{Q(T, L)} - 2. \tag{21}$$

This quantity is a linear combination of Q and Q^{-1}. It is easily seen that regardless of the form of $f(L)$, the leading correction of the universal ratio is reduced from $O(f(L))$ to $O(f(L)^2)$ if Q_∞ is chosen as the exact universal ratio:

$$
\begin{aligned}
S(T_c, L) &= \frac{1}{Q_\infty} Q(T_c, L) + Q_\infty \frac{1}{Q(T_c, L)} - 2 \\
&= \frac{Q_\infty + f(L)}{Q_\infty} + \frac{1}{1 + \frac{1}{Q_\infty} f(L)} - 2 \\
&\simeq \frac{f(L)}{Q_\infty} - \frac{f(L)}{Q_\infty} + \left(\frac{1}{Q_\infty} f(L)\right)^2 \\
&= O(f(L)^2).
\end{aligned}
\tag{22}
$$

In our analysis, we use the following self-combined Binder ratios:

$$S_{\text{MF}}(T, L) = \frac{1}{Q_{\text{MF}}} Q(T, L) + Q_{\text{MF}} \frac{1}{Q(T, L)} - 2, \tag{23}$$

$$S_{\text{SR}}(T, L) = \frac{1}{Q_{\text{SR}}} Q(T, L) + Q_{\text{SR}} \frac{1}{Q(T, L)} - 2, \tag{24}$$
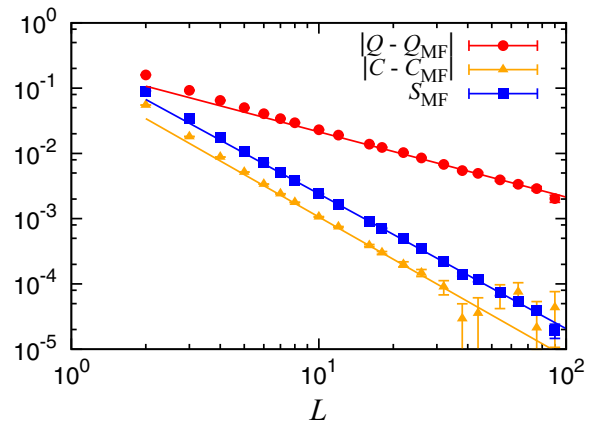

FIG. 1. Convergence of the conventional Binder ratio (red circles), Q, the combined Binder ratio (orange triangles), C, and the self-combined Binder ratio (blue squares), S_{MF}, at the critical point for the fully connected model. The conventional Binder ratio converges to Q_{MF} as $\sim L^{-1}$, while the combined Binder ratio and the self-combined Binder ratio converge as $\sim L^{-2}$ since the leading correction term is eliminated.
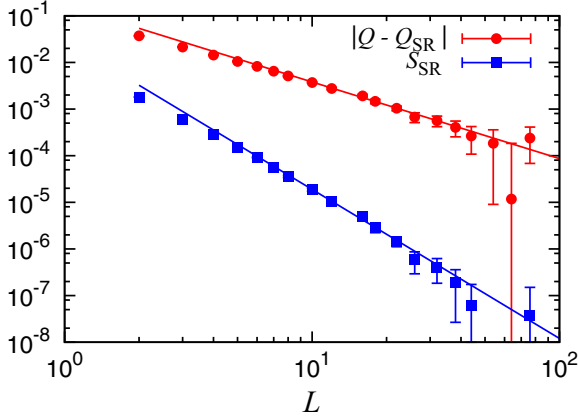
FIG. 2. Convergence of the conventional Binder ratio (red circles), Q, and the self-combined Binder ratio (blue squares), S_{SR} at the critical point for the nearest-neighbor model. The conventional Binder ratio converges to Q_{SR} as $\sim L^{-1.6}$, while the self-combined Binder ratio converges as $\sim L^{-3.2}$.

where $Q_{MF} = 0.456\,947$ and $Q_{SR} = 0.856\,216$ are the universal ratio of the mean-field universality [21] and the short-range universality [29], respectively. The former, $S_{MF}(T,L)$, converges to zero at the critical point for the mean-field universality class, and the latter, $S_{SR}(T,L)$, does so for the short-range universality class. Both should exhibit faster convergence than the conventional Binder ratio, $Q(T,L)$, since the leading correction is eliminated.

In Figs. 1 and 2, we compare the convergence of the conventional Binder ratio, the combined Binder ratio, and the self-combined Binder ratio to the limiting values for the fully connected model and the nearest-neighbor model in order to demonstrate the effectiveness of our new quantities. For both models, the (self-)combined Binder ratios converge much faster, in double powers, than the conventional Binder ratio. Again note that the combined Binder ratio, $C(T,L)$, is available only for the mean-field universality class and not for the short-range case. We will apply these combined quantities to the phase transition of the Ising model with the algebraically decaying interaction.

V. RESULTS

By means of the Fukui-Todo cluster method, a Monte Carlo simulation was performed on a two-dimensional $L \times L$ square lattice up to $L = 4096$ for $\sigma = 0.8, 0.9, 1.0, \ldots, 1.75, 1.9, 2.0$. Periodic boundary conditions were imposed, and the effect of the mirror images was taken into account by the generalized Ewald summation (Appendix A). The thermal averages of the moments of magnetization $\langle m^{\alpha} \rangle$ ($\alpha = 2, 4, \ldots$) were calculated using an improved estimator (Appendix B). Measurement of physical quantities are performed for 16 384 Monte Carlo steps, which is sufficiently longer than the integrated autocorrelation time, e.g., $\tau_{int} = 4.3$ and 4.0 for $\langle m^2 \rangle$ and $\langle m^4 \rangle$, respectively, at the critical point for $L = 4096$ and $\sigma = 1.75$. Before measurement, we discard 128 Monte Carlo steps. We have also confirmed that 128 Monte Carlo steps is sufficiently longer than the exponential autocorrelation time,

that is, there is no statistically significant difference between the measurement with 128 Monte Carlo thermalization steps and that with 256 Monte Carlo thermalization steps at the critical point for the largest system size.

A. Critical temperature

The critical temperature, T_c, was estimated by finite-size scaling of the Binder ratio. First, we estimated the critical temperature for each system size, $T_c(L)$, as the crossing point of the conventional Binder ratios of system size L and $2L$ ($L = 64, 128, 256, 512, 1024, 2048$). The crossing point is estimated using the Bayesian scaling analysis [30,31]. Then, we extrapolated the value in the thermodynamic limit by assuming the following form:

$$T_c(L) = T_c + aL^{-b}, \tag{25}$$

where the exponent b is related to the correction-to-scaling exponent, ω, as $1/\nu + \omega$. We observed that the value of b takes a larger value in the intermediate regime, as reported in Ref. [15]. Its precise estimation, however, is quite difficult even with the precision of the present simulation.

The critical temperature obtained for each σ is summarized in Table IV. We confirmed that the extrapolation assuming Eq. (25) produces estimates for the critical temperatures that agree with the values for the largest system size within the error bar. The estimation from the self-combined Binder ratio (crossing point) is also consistent with the result in Table IV. In the table, the normalized critical temperature is also listed, which is defined as $\tilde{T}_c = T_c/\tilde{J}$ with $\tilde{J} = \sum_{i \neq j} J_{ij}/N$, the sum of coupling constants connecting a single site to all the other sites. One can see that the normalized critical temperature, $\tilde{T}_c$, increases slowly as σ decreases. This shift of $\tilde{T}_c$ can be interpreted as a suppression of fluctuations due to the increase of the effective dimension.

TABLE IV. σ dependence of the critical temperature, T_c, and the normalized critical temperature, $\tilde{T}_c$. The exact results for the fully connected model (FC) and the nearest-neighbor model (NN) are also included.

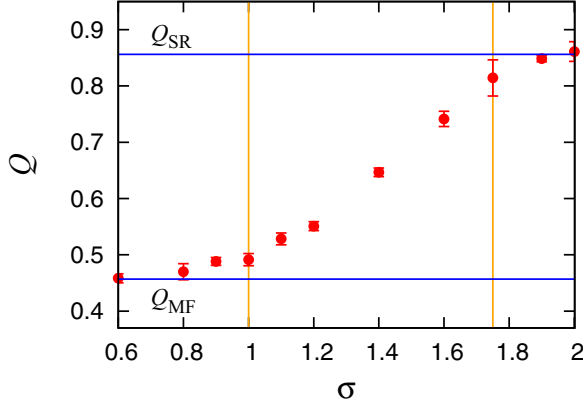| σ	T_c	$\tilde{T}_c$
0 (FC)	1	1
0.6	12.555(1)	0.954033(81)
0.8	9.76500(9)	0.923492(9)
0.9	8.80870(32)	0.906553(33)
1.0	8.03009(7)	0.888911(8)
1.1	7.38232(41)	0.870847(49)
1.2	6.83425(15)	0.852617(19)
1.4	5.95819(12)	0.816679(16)
1.6	5.29318(24)	0.782835(36)
1.75	4.89500(12)	0.759570(19)
1.9	4.56406(12)	0.738536(19)
2.0	4.37427(14)	0.725805(24)
∞ (NN)	2.269185	0.5672963

FIG. 3. σ dependence of the conventional Binder ratio at the critical point. The horizontal blue lines denote $Q_{\mathrm{MF}} = 0.456\,947$ [21] and $Q_{\mathrm{SR}} = 0.856\,216$ [29], respectively. The vertical orange lines denote the critical decay exponents $\sigma = 1$ and 7/4 predicted by Sak [3].

B. Binder ratio at critical temperature

Next, let us discuss the universality class of the phase transition by using the Binder ratio at the critical temperature. As we have already discussed in Sec. I, three different regions are expected: the mean-field, the intermediate, and the short-range regime. We will focus on the boundary, the critical decay exponent, separating the mean-field and the intermediate regimes, and the intermediate and the short-range regimes.

We calculated the Binder ratio at the critical temperature (Table IV) for each σ and L, and we extrapolated the value in the thermodynamic limit by assuming the following form:

$$Q(T_{\mathrm{c}}, L) = Q_{\infty} + aL^{-b} \tag{26}$$

for each σ, where a and b are σ-dependent fitting parameters.

In Fig. 3, the universal ratio of the conventional Binder ratio, Q, is plotted as a function of σ. The extrapolated values of Q are consistent with Q_{MF} in the cases for $\sigma = 0.6$ and 0.8, and with Q_{SR} for $\sigma = 1.9$ and 2. Meanwhile, the values deviate from Q_{MF} or Q_{SR} even outside the region $1 < \sigma < 7/4$, which is similar to the Monte Carlo result of Picco [11] and in contradiction to the conclusion by Sak [3]. We will show below, however, that this deviation and the smooth change are artifacts due to strong corrections to scaling.

Next, we examine the behavior of the self-combined Binder ratio. In Fig. 4, S_{MF} [Eq. (23)] is plotted as a function of σ, which has smaller corrections if the transition belongs to the mean-field universality class. In contrast to the conventional Binder ratio, S_{MF} becomes zero within the error bar for $\sigma \leqslant 1$. Moreover, it is observed that S_{MF} grows as $\sim(\sigma - 1)^2$ for $\sigma > 1$. Thus, we conclude that the transition belongs to the mean-field universality for $\sigma \leqslant 1$, and the conventional Binder ratio changes linearly as $|Q - Q_{\mathrm{MF}}| \sim (\sigma - 1)$ for $\sigma > 1$; i.e., the critical decay exponent between the mean-field and the intermediate regimes is 1, and Q (probably the critical exponents as well) is nonanalytic at $\sigma = 1$.

The boundary between the intermediate and the short-range regimes was investigated precisely with use of the self-combined Binder ratio, S_{SR} [Eq. (24)], as shown in Fig. 5. In a similar way to the previous case, S_{SR} decreases as $\sim(7/4 - \sigma)^2$
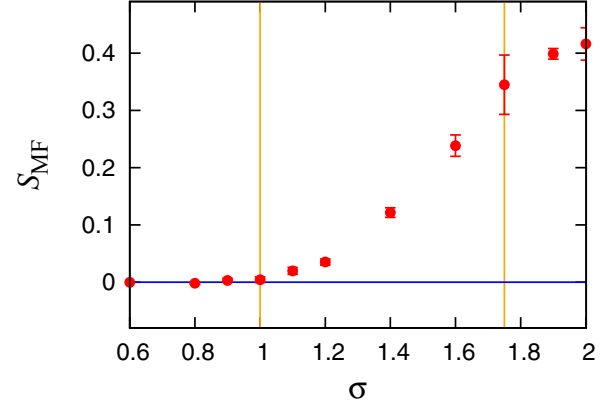

FIG. 4. σ dependence of the self-combined Binder ratio, S_{MF}, at the critical temperature. The vertical orange lines denote the critical decay exponents $\sigma = 1$ and 7/4 predicted by Sak [3].

for $\sigma < 7/4$ and becomes zero for $\sigma \geqslant 7/4$. Thus, we conclude that the critical decay exponent is $\sigma = 7/4$.

The apparent deviation of the conventional Binder ratio from the mean-field and short-range values at $\sigma = 1$ and 7/4, respectively, is due to the existence of strong (likely logarithmic [2,15,18]) corrections at the critical decay exponents. Indeed, the nearest-neighbor model exhibits logarithmic correction to scaling at the upper critical dimension ($d = 4$) [17]. In Figs. 6 and 7, we compare the system-size dependence of the conventional Binder ratio, the combined Binder ratio (only for $\sigma = 1$), and the self-combined Binder ratio for $\sigma = 1$ and 7/4, respectively. We observe that in both cases, the combined or self-combined Binder ratio converges to zero smoothly. On the other hand, the conventional Binder ratio has a stronger size dependence than the combined Binder ratios, which yields large error bars in the extrapolated values (open symbols). This observation indicates that the conventional Binder ratio presumably suffers from logarithmic-type corrections, while the (self-)combined Binder ratio is free from the strong corrections. In other words, we successfully remove the leading corrections of the conventional Binder ratio by considering the appropriate combination. Note that the
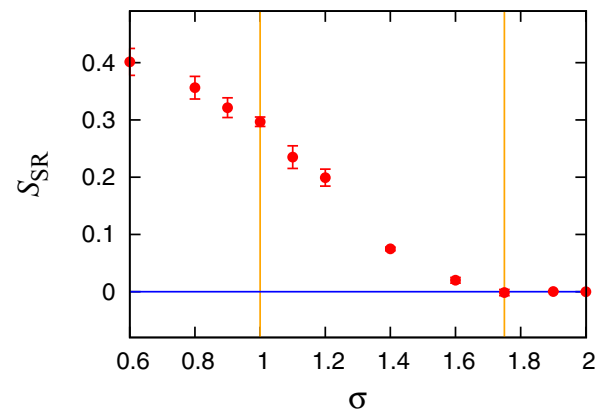

FIG. 5. σ dependence of the self-combined Binder ratio, S_{SR}, at the critical temperature. The vertical orange lines denote the critical decay exponents $\sigma = 1$ and 7/4 predicted by Sak [3].
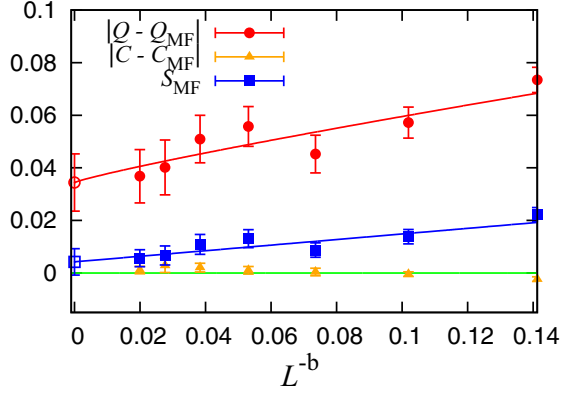
FIG. 6. System-size dependence of the conventional Binder ratio (Q with red circles), the combined Binder ratio (C with orange triangles), and the self-combined Binder ratio (S_{MF} with blue squares) at $\sigma = 1$. Open symbols denote the extrapolated values to the thermodynamic limit by the fit to a function, $A + aL^{-b}$, where A, a, and b are fitting parameters. The least-squares fitting yields $b \simeq 0.41$ and 0.47 for Q and S_{MF}, respectively. The x axis is taken as L^{-b} with $b = 0.41$.

combined and the self-combined Binder ratios have smaller error bars than the conventional Binder ratio. It is expected that the statistical fluctuations of the terms of the combined quantities cancel each other out in the linear combination.

Finally, it is quite interesting to see, in Fig. 6, that the combined Binder ratio [Eq. (19)] has even smaller corrections than the self-combined Binder ratio at $\sigma = 1$. The behavior of the conventional Binder ratio (red circles in Fig. 6) indicates that the leading correction term might have a different exponent (smaller than $1/2$) and a quite different form from Eq. (15). In such a case, Eq. (19) with coefficient (20) usually cannot eliminate the leading correction. The reason for this accidental cancellation is not clear at the moment. It remains a future problem.
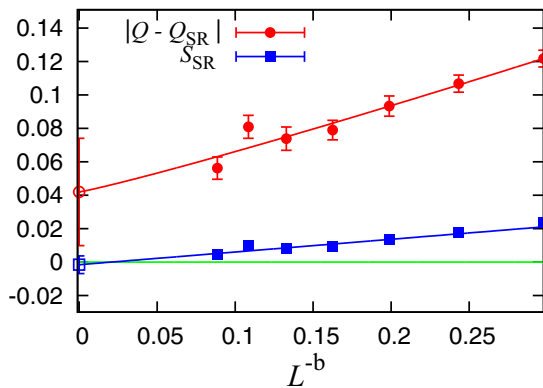

FIG. 7. System-size dependence of the conventional Binder ratio (Q with red circles) and the self-combined Binder ratio (S_{SR} with blue squares) at $\sigma = 7/4$. Open symbols denote the extrapolated values to the thermodynamic limit by the fit to a function, $A + aL^{-b}$, where A, a, and b are fitting parameters. The least-squares fitting yields $b \simeq 0.32$ and 0.29 for Q and S_{SR}, respectively. The x axis is taken as L^{-b} with $b = 0.32$.

VI. CONCLUSION

We have performed large-scale Monte Carlo simulations of the two-dimensional Ising model with algebraically decaying long-range interaction, and we clarified the universality-regime boundaries that have been a subject of debate for decades. To overcome the difficulties that make conventional analysis ineffective, we utilized several important techniques: the $O(N)$ Fukui-Todo cluster algorithm (Sec. III), the (self-) combined Binder ratio (Sec. IV), the generalized Ewald summation (Appendix A), and a generalization of the improved estimator for higher-order moments of magnetization (Appendix B). We conclude that in two dimensions, the lower and upper critical decay exponents are $\sigma = 1$ and $7/4$, respectively, which is consistent with the renormalization-group prediction by Sak [3] but is contrary to the recent Monte Carlo and renormalization studies by Picco [11] and Blanchard *et al.* [12]. The reason for the discrepancy is expected to be the strong (logarithmic) correction-to-scaling effect near the critical decay exponents [18]. We have observed that the logarithmic corrections hamper the standard analysis using the conventional Binder ratio. Nevertheless, our (self-) combined Binder ratio removes the leading corrections of the conventional quantity and allows for the reliable identification of the universality class.

The "self-combined" technique proposed in the present paper does not require a concrete expression of the correction terms. It should be noted, however, that a precise value of the universal ratio in the thermodynamic limit is needed beforehand to apply the proposed method to identify the universality class of a given system. Meanwhile, the present "self-combined" technique is quite powerful to test whether a phase transition belongs to some well-known universality class or not, as demonstrated in the present paper, since the leading correction terms are automatically eliminated as long as the correct limiting value is used. This property is expected to be useful not only for the present case but also for a wide range of problems, especially for the case with logarithmic corrections. The effectiveness of our approach in other problems needs to be investigated in the future.

APPENDIX A: GENERALIZED EWALD SUMMATION

In the simulation of systems with long-range interaction under periodic boundary conditions, we generally need to take into account interactions from mirror-image cells, which are imaginary systems across the periodic boundaries, in order to reduce strong finite-size corrections. The interaction between

S_i and S_j is thus expressed as

$$\mathcal{H}_{ij} = -\sum_{\vec{v}} \frac{1}{|\vec{L} \cdot \vec{v} + \vec{r}_i - \vec{r}_j|^{d+\sigma}} S_i S_j, \qquad \text{(A1)}$$

where $\vec{L} = (L_1, L_2, \ldots, L_d)$ denotes the size of the hypercubic system, and $\vec{v} = (v_1, v_2, \ldots, v_d)$ with $v_\alpha = 0, \pm 1, \pm 2, \ldots$ ($\alpha = 1, 2, \ldots, d$) represents the indices of image cells. In the following, we consider only the case in which $\sigma > 0$. The summation in Eq. (A1) is taken for all the image cells. The simplest way to get an approximate value of Eq. (A1) is by truncating the summation up to some threshold, $v_{\max}$, but this does not work well in practice because the summation of an algebraically decaying function converges very slowly. The Ewald-summation technique [34,35] is an efficient approach to calculate the contribution from image cells much faster [36,37]; the summation is broken into two parts—the short-range term and the long-range term—and taken separately in real space and reciprocal space, respectively. Although the Ewald summation is usually formulated only for integer exponents, $\sigma = 0, 1, 2, \ldots$, such as the Coulomb interaction and the dipole interaction, here we generalize the Ewald summation for an exponent of arbitrary positive real numbers.

Let us consider the potential of the following form:

$$\phi_m(i,j) = \sum_{\vec{v}} \frac{1}{|\vec{r}|^m}, \qquad \text{(A2)}$$

where $m = d + \sigma$ and $\vec{r} = \vec{r}(\vec{v}, \vec{r}_i, \vec{r}_j) \equiv \vec{L} \cdot \vec{v} + \vec{r}_i - \vec{r}_j$. We separate Eq. (A2) into two terms by using the Γ function:

$$\begin{aligned}
\phi_m(i,j) &= \sum_{\vec{v}} \frac{1}{\Gamma(m/2)} \int_0^\infty \frac{1}{|\vec{r}|^m} t^{\frac{m}{2}-1} e^{-t} dt \\
&= \sum_{\vec{v}} \left[\frac{1}{\Gamma(m/2)} \int_{(\kappa|\vec{r}|)^2}^\infty \frac{1}{|\vec{r}|^m} t^{\frac{m}{2}-1} e^{-t} dt \right. \\
&\quad \left. + \frac{2}{\Gamma(m/2)} \int_0^\kappa \rho^{m-1} e^{-|\vec{r}|^2 \rho^2} d\rho \right] \\
&= \phi_m^{(1)}(i,j) + \phi_m^{(2)}(i,j). \qquad \text{(A3)}
\end{aligned}$$

Here, $\Gamma(x)$ denotes the gamma function:

$$\Gamma(x) = \int_0^\infty t^{x-1} e^{-t} dt, \qquad \text{(A4)}$$

κ is an arbitrary positive real number,

$$\phi_m^{(1)}(i,j) = \sum_{\vec{v}} \frac{1}{\Gamma(m/2)} \frac{1}{|\vec{r}|^m} \int_{(\kappa|\vec{r}|)^2}^\infty t^{\frac{m}{2}-1} e^{-t} dt \qquad \text{(A5)}$$

represents the short-range term, and

$$\phi_m^{(2)}(i,j) = \sum_{\vec{v}} \frac{2}{\Gamma(m/2)} \int_0^\kappa \rho^{m-1} e^{-|\vec{r}|^2 \rho^2} d\rho \qquad \text{(A6)}$$

represents the long-range term. Note that in Eq. (A6) we have replaced the integration variable t by $(|\vec{r}|\rho)^2$.

Next, we transform Eq. (A6) from the integration in real space into that in reciprocal space. Let us consider the two-dimensional case, i.e., $d = 2$, $\vec{L} = (L_x, L_y)$, $v = (v_x, v_y)$,

$\vec{r}_i = (r_{ix}, r_{iy})$, etc. We factor $\sum_{\vec{v}} e^{-|\vec{r}|^2 \rho^2}$ in Eq. (A6) into the two components for each coordinate axis as

$$G(\vec{r}_i, \vec{r}_j) = \sum_{\vec{v}} e^{-|\vec{r}|^2 \rho^2} = G_x(r_{ix}, r_{jx}) G_y(r_{iy}, r_{jx}), \qquad \text{(A7)}$$

where

$$G_x(r_{ix}, r_{jx}) = \sum_{v_x=-\infty}^\infty \exp[-(L_x v_x + r_{ix} - r_{jx})^2 \rho^2] \qquad \text{(A8)}$$

and

$$G_y(r_{iy}, r_{jy}) = \sum_{v_y=-\infty}^\infty \exp[-(L_y v_y + r_{iy} - r_{jy})^2 \rho^2]. \qquad \text{(A9)}$$

Then, Eq. (A8) is rewritten by taking the Fourier transform on r_{ix} as

$$G_x(r_{ix}, r_{jx}) = \sum_{h_x=-\infty}^\infty \frac{1}{L_x} A_x(h_x, r_{jx}) \exp\left(i \frac{2\pi h_x}{L_x} r_{ix} \right), \qquad \text{(A10)}$$

where

$$\begin{aligned}
A_x(h_x, r_{jx}) &= \int_0^{L_x} G_x(r_{ix}, r_{jx}) \exp\left(-i \frac{2\pi h_x}{L_x} r_{ix} \right) dr_{ix} \\
&= \sum_{v_x} \int_{L_x v_x - r_{jx}}^{L_x(v_x+1)-r_{jx}} \exp\left[-\xi^2 \rho^2 \right. \\
&\quad \left. - i \frac{2\pi h_x}{L_x} \xi + i 2\pi h_x v_x - i \frac{2\pi h_x}{L_x} r_{jx} \right] d\xi \\
&= \int_{-\infty}^\infty \exp\left[-\xi^2 \rho^2 - i \frac{2\pi h_x}{L_x} \xi - i \frac{2\pi h_x}{L_x} r_{jx} \right] d\xi \qquad \text{(A11)}
\end{aligned}$$

with $\xi = L_x v_x + r_{ix} - r_{jx}$. Note that $\exp(i 2\pi h_x v_x)$ vanishes because $h_x v_x$ takes integral values. Performing the Gaussian integration then yields

$$A_x(h_x, r_{jx}) = \frac{\sqrt{\pi}}{\rho} \exp\left(-\frac{\pi^2 h_x^2}{\rho^2 L_x^2} - i \frac{2\pi h_x}{L_x} r_{jx} \right). \qquad \text{(A12)}$$

Next, by using Eq. (A10) with Eq. (A12) and a similar expression for $G_y(r_{iy}, r_{jy})$, Eq. (A7) is expressed as

$$\begin{aligned}
G(\vec{r}_i, \vec{r}_j) = \sum_{h_x, h_y} \frac{\pi}{L_x L_y \rho^2} &\exp\left[-\frac{\pi^2}{\rho^2} \left(\frac{h_x^2}{L_x^2} + \frac{h_y^2}{L_y^2} \right) \right. \\
&\left. + i 2\pi \left(\frac{h_x}{L_x} (r_{ix} - r_{jx}) + \frac{h_y}{L_y} (r_{iy} - r_{jy}) \right) \right]. \qquad \text{(A13)}
\end{aligned}$$

Introducing $\vec{k} = \left(\frac{h_x}{L_x}, \frac{h_y}{L_y} \right)$, Eq. (A13) is further simplified as

$$\begin{aligned}
G(\vec{r}_i, \vec{r}_j) = \sum_{\vec{k}} \frac{\pi}{L_x L_y \rho^2} &\exp\left[-\frac{\pi^2}{\rho^2} |\vec{k}|^2 \right] \\
&\times \{\cos[2\pi \vec{k} \cdot (\vec{r}_i - \vec{r}_j)] + i \sin[2\pi \vec{k} \cdot (\vec{r}_i - \vec{r}_j)]\}. \qquad \text{(A14)}
\end{aligned}$$

Here, $\exp[-\frac{\pi^2}{\rho^2}|\vec{k}|^2]$ and $\cos[2\pi\vec{k}\cdot(\vec{r}_i-\vec{r}_j)]$ are even functions of $\vec{k}$. On the other hand, $\sin[2\pi\vec{k}\cdot(\vec{r}_i-\vec{r}_j)]$ is an odd function. Therefore, $\sin[2\pi\vec{k}\cdot(\vec{r}_i-\vec{r}_j)]$ and $\sin[2\pi(-\vec{k})\cdot(\vec{r}_i-\vec{r}_j)]$ are counterbalanced if summation is taken for all $\vec{k}$.

Extension of the above argument to arbitrary dimensions is straightforward. For the d-dimensional case, Eq. (A14) should be replace by

$$G(\vec{r}_i,\vec{r}_j) = \frac{\pi^{d/2}}{V\rho^d}\sum_{\vec{k}}\exp\left[-\frac{\pi^2}{\rho^2}|\vec{k}|^2\right]\cos[2\pi\vec{k}\cdot(\vec{r}_i-\vec{r}_j)],$$

(A15)

where $V=\Pi_{\alpha=1}^d L_\alpha$ is the volume of the system. The long-range term (A6) is finally expressed as

$$\phi_m^{(2)}(i,j) = \frac{2\pi^{d/2}}{\Gamma(m/2)V}\sum_{\vec{k}}\cos[2\pi\vec{k}\cdot(\vec{r}_i-\vec{r}_j)]$$

$$\times\int_0^\kappa \rho^{m-1-d}\exp\left[-\frac{\pi^2}{\rho^2}|\vec{k}|^2\right]d\rho$$

$$= \frac{2\pi^{d/2}}{\Gamma(m/2)V}\sum_{\vec{k}}\cos[2\pi\vec{k}\cdot(\vec{r}_i-\vec{r}_j)]$$

$$\times\frac{1}{2}(\pi|\vec{k}|)^{m-d}\int_{\frac{\pi^2|\vec{k}|^2}{\kappa^2}}^\infty t^{-\frac{1}{2}(m-d)-1}e^{-t}dt. \quad (A16)$$

In summary, the Ewald summation for generic exponent σ is expressed as Eq. (A2) with the short-range term (A5) and the long-range term (A16). The terms in Eqs. (A5) and (A16) become small quite rapidly as $|\vec{v}|$ and $|\vec{k}|$ increase, respectively, due to the presence of the exponential functions. Note that the choice of the crossover parameter κ affects the speed of convergence of the summations over $\vec{v}$ and $\vec{k}$ (or $\vec{h}$). We find empirically that $\kappa=2/L$ is a reasonable choice, by which both summations converge in double precision for $\max(|v_x|,|v_y|)\leqslant 4$ and $\max(|h_x|,|h_y|)\leqslant 4$.

The integrals in Eqs. (A5) and (A16) are calculated numerically. These integrals are known as the (upper) incomplete Γ function, which is defined as

$$\Gamma(s,x)=\int_x^\infty t^{s-1}e^{-t}dt. \quad (A17)$$

Equations (A5) and (A16) are expressed by the incomplete Γ function as

$$\phi_m^{(1)}(i,j)=\sum_{\vec{v}}\frac{1}{\Gamma(m/2)}\frac{1}{|\vec{r}|^m}\Gamma\left(\frac{m}{2},(\kappa|\vec{r}|)^2\right), \quad (A18)$$

$$\phi_m^{(2)}(i,j)=\frac{2\pi^{d/2}}{\Gamma(m/2)V}\sum_{\vec{k}}\cos[2\pi\vec{k}\cdot(\vec{r}_i-\vec{r}_j)]$$

$$\times\frac{1}{2}(\pi|\vec{k}|)^{m-d}\Gamma\left(-\frac{1}{2}(m-d),\frac{\pi^2|\vec{k}|^2}{\kappa^2}\right), \quad (A19)$$

respectively.

In the present simulation, we calculated the incomplete Γ function numerically by the Boost C++ library [38]. The function (A17), however, is defined only for positive real s in the library. In the case of negative s, we used the following recursion formula obtained by integration by parts:

$$\Gamma(s,x)=\int_x^\infty t^{s-1}e^{-t}dt$$

$$=\left[\frac{1}{s}t^s e^{-t}\right]_x^\infty+\int_x^\infty\frac{1}{s}t^s e^{-t}dt$$

$$=-\frac{1}{s}x^s e^{-x}+\frac{1}{s}\Gamma(s+1,x)$$

$$=-\frac{1}{s}x^s e^{-x}-\frac{1}{s(s+1)}x^{s+1}e^{-x}$$

$$+\frac{1}{s(s+1)}\Gamma(s+2,x)$$

$$\vdots$$

$$=-\sum_{i=1}^n\left\{x^{s+i-1}e^{-x}\prod_{j=1}^i\left(\frac{1}{s+j-1}\right)\right\}$$

$$+\prod_{i=1}^n\left(\frac{1}{s+i-1}\right)\Gamma(s+n,x), \quad (A20)$$

where $n=-\lfloor s\rfloor$. Note that this recursion formula breaks down when σ is an even (positive) integer since $-(m-d)/2=-\sigma/2$ becomes a negative integer. The denominator in Eq. (A20) then becomes zero during the recursion. For even σ, we stop the recursion when the first argument of the incomplete Γ function becomes zero, and we use

$$\Gamma(0,x)=\int_x^\infty t^{-1}e^{-t}dt=-\mathrm{Ei}(-x), \quad (A21)$$

where $\mathrm{Ei}(-x)$ is the exponential integral.

APPENDIX B: IMPROVED ESTIMATOR

In the cluster algorithm Monte Carlo methods, so-called the improved estimators for physical quantities are available, which are defined in terms of the cluster configuration instead of the spin configuration. Some improved estimators can drastically reduce the asymptotic variance of physical quantities because they take the average of a number of spin configurations generated from a cluster configuration automatically. In the present work, we used the improved estimators for measuring the moments of magnetization, i.e., $\langle m^2\rangle$, $\langle m^4\rangle$, $\langle m^6\rangle$, ..., to calculate the (combined) Binder ratios.

Let us consider a snapshot of graph configuration g composed of k clusters, and let $n_1,n_2,\ldots,n_k$ be the number of spins included in each cluster. We define $m^\alpha(g)$ as an average of m^α over all possible 2^k different spin configurations that

can be generated by flipping k clusters independently:

$$m^\alpha(g) = \frac{1}{2^k} \sum_{s_1,\ldots,s_k} \left(\sum_i^k n_i s_i \right)^\alpha$$

$$= \frac{1}{2^k} \{ (+n_1 + n_2 + \cdots + n_k)^\alpha$$
$$+ (-n_1 + n_2 + \cdots + n_k)^\alpha$$
$$+ (+n_1 - n_2 + \cdots + n_k)^\alpha$$
$$\vdots$$
$$+ (-n_1 - n_2 - \cdots - n_k)^\alpha \}, \quad \text{(B1)}$$

where $s_i = \pm 1$ denotes the spin direction of the ith cluster. In Eq. (B1), terms including an odd power of $n_1, n_2, \ldots, n_k$ are counterbalanced by other terms with the opposite sign. Hence we only have to consider the terms with even powers for all $\{n_i\}$. Thus, we can rewrite Eq. (B1) as

$$m^\alpha(g) = \frac{1}{2^k} 2^k (n_1 + n_2 + \cdots + n_k)^\alpha_{\text{even terms}}$$
$$= (n_1 + n_2 + \cdots + n_k)^\alpha_{\text{even terms}}. \quad \text{(B2)}$$

Now we assume that $m^\alpha(g)$ can be expressed as

$$m^\alpha(g) = \sum_p a_p \prod_{j \in p} C_j, \quad \text{(B3)}$$

with coefficients $\{a_p\}$ and

$$C_j = \sum_i^k n_i^j. \quad \text{(B4)}$$

The summation $\sum_p$ in Eq. (B3) is taken over all possible partitions of α into a set of even integers $\{j\}$. Nevertheless, we do not need to consider the combinations with odd j since they do not contribute after taking the average over the spin configurations, as already mentioned.

We introduce a simple way to obtain $\{a_p\}$ by expanding the right-hand side of Eqs. (B2) and (B3), and comparing their coefficients.

1. Second moment: $m^2(g)$

To determine the improved estimator for the second moment of magnetization, it is enough to consider a graph configuration composed of only one cluster. In this case, Eq. (B2) becomes

$$m^2(g) = n_1^2. \quad \text{(B5)}$$

On the other hand, Eq. (B3) is expressed as

$$m^2(g) = a_1 \sum_i^k n_i^2 = a_1 n_1^2. \quad \text{(B6)}$$

By comparing Eqs. (B5) and (B6), we obtain

$$a_1 = 1. \quad \text{(B7)}$$

The improved estimator $m^2(g)$ is thus given by

$$m^2(g) = C_2. \quad \text{(B8)}$$

2. Fourth moment: $m^4(g)$

Consider a graph configuration composed of two clusters. From Eq. (B2), we obtain

$$m^4(g) = (n_1 + n_2)^4_{\text{even terms}}$$
$$= (n_1^4 + n_2^4) + 6n_1^2 n_2^2. \quad \text{(B9)}$$

On the other hand, Eq. (B3) is expressed as

$$m^4(g) = a_1 C_4 + a_2 C_2^2$$
$$= (a_1 + a_2)(n_1^4 + n_2^4) + 2a_2 n_1^2 n_2^2. \quad \text{(B10)}$$

By comparing Eqs. (B9) and (B10), we obtain

$$a_1 = -2,$$
$$a_2 = 3. \quad \text{(B11)}$$

The improved estimator $m^4(g)$ is thus given by

$$m^4(g) = -2C_4 + 3C_2^2. \quad \text{(B12)}$$

3. Sixth moment: $m^6(g)$

Consider a graph configuration composed of three clusters. From Eq. (B2), we obtain

$$m^6(g) = (n_1 + n_2 + n_3)^6_{\text{even terms}}$$
$$= (n_1^6 + n_2^6 + n_3^6)$$
$$+ 15\{n_1^4(n_2^2 + n_3^2) + n_2^4(n_1^2 + n_3^2) + n_3^4(n_1^2 + n_2^2)\}$$
$$+ 90n_1^2 n_2^2 n_3^2. \quad \text{(B13)}$$

On the other hand, Eq. (B3) is expanded as

$$m^6(g) = a_1 C_6 + a_2 C_4 C_2 + a_3 C_2^3$$
$$= (a_1 + a_2 + a_3)(n_1^6 + n_2^6 + n_3^6)$$
$$+ (a_2 + 3a_3)\{n_1^4(n_2^2 + n_3^2) + n_2^4(n_1^2 + n_3^2)$$
$$+ n_3^4(n_1^2 + n_2^2)\}$$
$$+ 6a_3 n_1^2 n_2^2 n_3^2. \quad \text{(B14)}$$

By comparing Eqs. (B13) and (B14), we obtain

$$a_1 = 16,$$
$$a_2 = -30,$$
$$a_3 = 15. \quad \text{(B15)}$$

The improved estimator $m^6(g)$ is thus given by

$$m^6(g) = 16C_6 - 30C_4 C_2 + 15C_2^3. \quad \text{(B16)}$$

4. Eighth moment: $m^8(g)$

Consider a graph configuration composed of four clusters. From Eq. (B2), we obtain

$$m^8(g) = (n_1 + n_2 + n_3 + n_4)^8_{\text{even terms}}$$
$$= (n_1^8 + n_2^8 + n_3^8 + n_4^8) + 28 \sum_i n_i^6 \sum_{j \neq i} n_j^2$$
$$+ 420 \sum_i n_i^4 \sum_{j \neq i} n_j^2 \sum_{\ell \neq j, \ell \neq i} n_\ell^2 + 70 \sum_i n_i^4 \sum_{j \neq i} n_j^4$$
$$+ 2520 n_1^2 n_2^2 n_3^2 n_4^2. \quad \text{(B17)}$$

On the other hand, Eq. (B3) can be expanded as

$$
\begin{aligned}
m^8(g) &= a_1 C_8 + a_2 C_6 C_2 + a_3 C_4 C_2^2 + a_4 C_4^2 + a_5 C_2^4 \\
&= (a_1 + a_2 + a_3 + a_4 + a_5) \sum_i n_i^8 \\
&\quad + (a_2 + 2a_3 + 4a_5) \sum_i n_i^6 \sum_{j \neq i} n_j^2 \\
&\quad + (2a_3 + 12a_5) \sum_i n_i^4 \sum_{j \neq i} n_j^2 \sum_{\ell \neq j, \ell \neq i} n_\ell^2 \\
&\quad + (2a_3 + 2a_4 + 6a_5) \sum_i n_i^4 \sum_{j \neq i} n_j^4 \\
&\quad + 24 a_5 n_1^2 n_2^2 n_3^2 n_4^2.
\end{aligned}
\tag{B18}
$$

By comparing Eqs. (B17) and (B18), we obtain

$$
\begin{aligned}
a_1 &= -272, \\
a_2 &= 448, \\
a_3 &= -420, \\
a_4 &= 140, \\
a_5 &= 105.
\end{aligned}
\tag{B19}
$$

The improved estimator $m^8(g)$ is thus given by

$$
\begin{aligned}
m^8(g) = {}&-272 C_8 + 448 C_6 C_2 - 420 C_4 C_2^2 \\
&+ 140 C_4^2 + 105 C_2^4.
\end{aligned}
\tag{B20}
$$

[1] F. J. Dyson, Commun. Math. Phys. **12**, 91 (1969).
[2] M. E. Fisher, S.-K. Ma, and B. G. Nickel, Phys. Rev. Lett. **29**, 917 (1972).
[3] J. Sak, Phys. Rev. B **8**, 281 (1973).
[4] C. Kraemer, N. Nikseresht, J. O. Piatek, N. Tsyrulin, B. D. Piazza, K. Kiefer, B. Klemke, T. F. Rosenbaum, G. Aeppli, C. Gannarelli, K. Prokes, A. Podlesnyak, T. Strässle, L. Keller, O. Zaharko, K. W. Krämer, and H. M. Rønnow, Science **336**, 1416 (2012).
[5] H. Prüser, P. E. Dargel, M. Bouhassoune, R. G. Ulbrich, T. Pruschke, S. Lounis, and M. Wenderoth, Nat. Commun. **5**, 5417 (2014).
[6] R. Landig, L. Hruby, N. Dogra, M. Landini, R. Mottl, T. Donner, and T. Esslinger, Nature (London) **532**, 476 (2016).
[7] K. Husimi, in *Proceedings of the International Conference of Theoretical Physics* (Science Council of Japan, Kyoto and Tokyo, 1953), p. 531.
[8] H. N. V. Temperley, Proc. Phys. Soc. **67**, 233 (1954).
[9] A. C. D. van Enter, Phys. Rev. B **26**, 1336 (1982).
[10] E. Luijten and H. W. J. Blöte, Phys. Rev. Lett. **89**, 025703 (2002).
[11] M. Picco, arXiv:1207.1018.
[12] T. Blanchard, M. Picco, and M. A. Rajabpour, Europhys. Lett. **101**, 56003 (2013).
[13] H. G. Katzgraber, D. Larson, and A. P. Young, Phys. Rev. Lett. **102**, 177205 (2009).
[14] R. A. Banos, L. A. Fernandez, V. Martin-Mayor, and A. P. Young, Phys. Rev. B **86**, 134416 (2012).
[15] M. C. Angelini, G. Parisi, and F. Ricci-Tersenghi, Phys. Rev. E **89**, 062120 (2014).
[16] N. Defenu, A. Trombettoni, and A. Codello, Phys. Rev. E **92**, 052113 (2015).
[17] E. Brézin, J. Phys. (France) **43**, 15 (1982).
[18] E. Brézin, G. Parisi, and F. Ricci-Tersenghi, J. Stat. Phys. **157**, 855 (2014).
[19] K. Fukui and S. Todo, J. Comp. Phys. **228**, 2629 (2009).
[20] H. Nishimori and G. Ortiz, *Elements of Phase Transition and Critical Phenomena* (Oxford University Press, Oxford, 2011).
[21] E. Luijten and H. W. J. Blöte, Int. J. Mod. Phys. C **6**, 359 (1995).
[22] Y. Tomita, J. Phys. Soc. Jpn. **78**, 014002 (2009).
[23] S. Todo and H. Suwa, J. Phys.: Conf. Ser. **473**, 012013 (2013).
[24] R. H. Swendsen and J. S. Wang, Phys. Rev. Lett. **58**, 86 (1987).
[25] C. M. Fortuin and P. W. Kasteleyn, Physica **57**, 536 (1972).
[26] N. Kawashima and J. E. Gubernatis, J. Stat. Phys. **80**, 169 (1995).
[27] D. P. Landau and K. Binder, *A Guide to Monte Carlo Simulations in Statistical Physics*, 2nd ed. (Cambridge University Press, Cambridge, 2005).
[28] S. Yasuda and S. Todo, Phys. Rev. E **88**, 061301(R) (2013).
[29] G. Kamieniarz and H. W. J. Blöte, J. Phys. A **26**, 201 (1993).
[30] K. Harada, Phys. Rev. E **84**, 056704 (2011).
[31] http://kenjiharada.github.io/BSA/.
[32] B. Bauer, L. D. Carr, H. G. Evertz, A. Feiguin, J. Freire, S. Fuchs, L. Gamper, J. Gukelberger, E. Gull, S. Guertler, A. Hehn, R. Igarashi, S. V. Isakov, D. Koop, P. N. Ma, P. Mates, H. Matsuo, O. Parcollet, G. Pawlowski, J. D. Picon, L. Pollet, E. Santos, V. W. Scarola, U. Schollwöck, C. Silva, B. Surer, S. Todo, S. Trebst, M. Troyer, M. L. Wall, P. Werner, and S. Wessel, J. Stat. Mech. (2011) P05001.
[33] http://alps.comp-phys.org/.
[34] P. P. Ewald, Ann. Phys. **369**, 253 (1921).
[35] N. Karasawa and W. A. Goddard, J. Chem. Phys. **93**, 7320 (1989).
[36] R. Kretschmer and K. Binder, Z. Phys. B **34**, 375 (1979).
[37] A. Ueda, *Computer Simulation* (Asakura, Tokyo, 1990) (in Japanese).
[38] http://www.boost.org/.